

## Main Manuscript for

### Signatures of muscle disuse in spaceflight and bed rest revealed by single muscle fiber proteomics.

Marta Murgia<sup>1,2\*</sup>, Stefano Ciciliot<sup>3,4</sup>, Nagarjuna Nagaraj<sup>5</sup>, Carlo Reggiani<sup>1,6</sup>, Stefano Schiaffino<sup>3</sup>, Martino V Franchi<sup>1</sup>, Rado Pišot<sup>6</sup>, Boštjan Šimunič<sup>6</sup>, Luana Toniolo<sup>1</sup>, Bert Blaauw<sup>1,3</sup>, Marco Sandri<sup>1,3</sup>, Gianni Biolo<sup>7</sup>, Martin Flück<sup>8</sup>, Marco V Narici<sup>1,6,9</sup> and Matthias Mann<sup>2,10\*</sup>.

<sup>1</sup> Department of Biomedical Sciences, University of Padova, Via Ugo Bassi, 58/B, 35131Padua, Italy

<sup>2</sup> Max-Planck-Institute of Biochemistry, Am Klopferspitz 18, 82152Martinsried, Germany

<sup>3</sup> Veneto Institute of Molecular Medicine, Via Orus 2, 35129 Padua, Italy

<sup>4</sup> Department of Molecular Medicine, University of Pavia, Via Forlanini 6, 27100 Pavia, Italy

<sup>5</sup> Bruker Daltonik, GmbH, Fahrenheitstr. 4, 28359 Bremen, Germany

<sup>6</sup> Science and Research Center Koper, Institute for Kinesiology Research, Garibaldijeva Street 1, 6000 Koper, Slovenia

<sup>7</sup> Clinical Department of Medical, Surgical and Health Sciences, Strada di Fiume 447, 34149 Trieste, Italy

<sup>8</sup> Department of Medicine, University of Fribourg, Chemin du Musee 5, 1700 Fribourg, Switzerland.

<sup>9</sup> CIR-MYO Myology Center, Viale G Colombo 3, 35121 Padua, Italy

<sup>10</sup> NNF Center for Protein Research, Faculty of Health Sciences, University of Copenhagen, Blegdamsvej 3B, building 6.1, 2200 Copenhagen, Denmark.

\*Correspondence: Marta Murgia and Matthias Mann.

**Email:** mmurgia@biochem.mpg.de, mmann@biochem.mpg.de

**Author Contributions:** Conceptualization MMu, MVN, SS, MS. Data curation MMu and NN. Formal Analysis MMu, NN, SC and GB. Funding acquisition MVN, MMu and MMA. Investigation MMu, SC, LT, CR, MVF. Methodology MVN, SS, RP, BS, MF. Project administration RP, BS. Resources MF, GB, BB, LT, RP, BS. Supervision MVF. Validation MMu. Visualization MMu, SC. Writing – original draft MMu, MVN, MMA. Writing – review & editing MMu, MVN, MMA, SS, CR, MF, MVF.

**Competing Interest Statement:** The authors declare no competing interests.

**Classification:** Biological Sciences, Biochemistry

**Keywords:** proteomics, skeletal muscle, single fibers, bed rest, microgravity, atrophy, astronauts

## Abstract

Astronauts experience dramatic loss of muscle mass, decreased strength and insulin resistance, despite performing daily intense physical exercise that would lead to muscle growth on Earth. Partially mimicking spaceflight, prolonged bed rest causes muscle atrophy, loss of force and glucose intolerance. To unravel the underlying mechanisms, we employed highly sensitive single fiber proteomics to detail the molecular remodeling caused by unloading and inactivity during bed rest and changes of the muscle proteome of astronauts before and after a mission on the International Space Station. Muscle focal adhesions, involved in fiber-matrix interaction and insulin receptor stabilization, are prominently downregulated in both bed rest and spaceflight and restored upon reloading. Pathways of anti-oxidant response increased strongly in slow but not in fast muscle fibers. Unloading alone upregulated markers of neuromuscular damage and the pathway controlling EIF5A hypusination. These proteomic signatures of mechanical unloading in muscle fiber subtypes contribute to disentangle the effect of microgravity from the pleiotropic challenges of spaceflight.

## Significance Statement

In the absence of mechanical loading, skeletal muscle undergoes atrophy with loss of strength and detrimental metabolic effects. We use mass spectrometry-based proteomics to compare single skeletal muscle fibers of healthy volunteers before and after ten days of continuous bed rest. In these multinucleated single cells, we find that protein complexes responsible for the interaction with the extracellular matrix and for force transmission are strongly downregulated in the unloading phase. Slow and fast fiber types undergo partially different changes. Our parallel proteomic analysis of muscle biopsies of astronauts before and after a six-month mission on the International Space Station highlights similar changes caused by lack of gravity despite daily exercise. We lay a molecular basis for countermeasures.

## Introduction

Human muscles are composed of three types of multinucleated single cells, the muscle fibers, named slow-type 1, fast-2A and fast-2X, with distinct contractile performance and metabolic profile ranging from slow/oxidative to fast/glycolytic. The expression of one specific isoform of myosin heavy chain (MYH) defines fiber type and is the main determinant of contractile properties. In addition, some fibers are mixed-type, expressing two MYH isoforms, mostly 1+2A and 2A+2X, at comparable levels (1).

In healthy humans, two days of immobilization are sufficient to trigger a loss of muscle mass of about 2% progressively increasing to 17% over the course of eight weeks (2, 3). The concomitant loss of muscle strength is proportionally greater than the actual decrease in muscle mass (4-6). At the cellular level, mechanical unloading causes marked alterations in single fiber morphological, histochemical, and mechanical properties (7-10). Muscle unloading or inactivity are accompanied by glucose intolerance and other detrimental effects on whole-body metabolism (11, 12).

At Earth gravity, these perturbations are fully reverted by physical activity (13). During spaceflight, astronauts experience consistent loss of muscle mass and strength despite daily sessions of intense exercise (5, 14, 15). Muscle atrophy is caused by the absence of gravitational loading and imposes an additional burden to the health of astronauts (16-18) on top of other challenges inherent to spaceflight, including ionizing radiation and disruption of circadian rhythms (19, 20).

Earth-bound models of disuse, such as bed rest, unilateral lower limb suspension or dry immersion, can dissect the effects of muscle unloading from the other environmental changes inherent to spaceflight (21, 22). These simulated microgravity models allow the sequential analysis of structural and functional changes at multiple time points, which has so far proved

impossible during spaceflights. In addition, rodents (23) and cell lines (24) subjected to spaceflight or parabolic flight are contributing an increasing body of mechanistic information.

With the perspective of human missions in deep space drawing near, mechanistic knowledge of the effects skeletal muscle unloading is essential for the development of countermeasures. Slow fibers, performing tasks of posture and tonic activity, and fast fibers, engaged in phasic movements requiring more force, have been shown to respond differently to disuse (18). The optimization of targeted countermeasures decelerating atrophy in astronauts would benefit from fiber type-resolved mechanistic knowledge of unloading-mediated atrophy. We previously applied mass spectrometry-based proteomics to single muscle fibers for the first time (25) and used this approach to detail the specific response of each fiber type to activity (26), and aging (27). In addition, this allowed us to reveal muscle fiber-intrinsic changes devoid of the contribution of other tissue components like blood vessels and interstitial cells. For muscle inactivity specifically, fibro-adipogenic progenitors and intramuscular fat infiltration might significantly alter the cell composition of whole muscle lysate (28).

Here, we analyzed 233 muscle fibers isolated from the biopsies of young healthy volunteers who underwent ten days of continuous bed rest without any muscle loading or physical activity. In parallel, we measured the muscle proteome of two astronauts, from biopsies taken before and after six months of permanence on the International Space Station (ISS) with daily exercise as countermeasure for unloading. We applied state-of-the-art trapped ion mobility spectrometry (TIMS) time of flight (TOF) quantitative mass spectrometry (MS)-based proteomics, which has recently led to the first measurement of a mononucleated single cell proteome (29).

We compare the remodeling of skeletal muscle caused by spaceflight and bed rest on Earth using the same proteomic workflow and quantification methods. Our study reveals proteomic signatures controlled by weight load in muscle, possibly contributing to insulin signaling and glucose tolerance. Our dataset is a resource to disentangle the direct effects of unloading and disuse of skeletal muscle from the consequences of other complex challenges of microgravity, such as changes in neural adaptations, altered muscle perfusion due to cardiovascular deconditioning, osteoarticular modifications and cosmic radiation (30-32).

## Results

### Proteomic workflow and single muscle fiber type assignment.

We dissected and analyzed by MS a total of 233 single muscle fibers from ten volunteers undergoing strict bed rest for ten days (Table S1). Muscle biopsies were taken immediately before bed rest (BR0), at day 5 (BR5) and 10 (BR10). We then examined whole muscle lysates of two astronauts who spent six months on the International Space Station (ISS), undergoing one muscle biopsy before and two after the mission. Our proteomic analysis quantified over 7500 proteins in the muscle fibers (2900 per single fiber on average) and 7100 in the whole muscle lysates of astronauts (Table S2-S3, Figure S1A). Over 93% of proteins were quantified at all three time points of bed rest and 65 % in all ten donors; in astronauts, 74% of proteins was quantified at three time points and 82% in both individuals (Figure S1B). This confirms the robustness and stability of our workflow and allows comprehensive systematic comparisons within and between our datasets.

Based on MS analysis of myosin heavy chain isoforms (MYH, see methods), we assigned 82 fiber types as pure slow-1, 56 as fast-2A and 25 as fast 2X. Fibers expressing less than the threshold percent of a single MYH isoform were defined as “mixed fibers” and assigned to the 1/2A and 2A/2X group according to the more abundant isoforms (Figure 1B). Other MYH isoforms were expressed with MS-intensities three orders of magnitude lower than the majority isoforms (Table S4). The proportion of fiber types collected at the three time points of bed rest showed only minor variations (Figure S1C). Comparing the proteomes of slow and

fast fiber types highlighted 470 proteins with significantly different expression between pure slow-1 and fast-2A fiber and 481 between Slow-1 and fast-2X (Figure S1D-E and Tables S5-S6). Myosin and troponin isoforms displayed the largest and most significant differences between fiber types, providing positive control

Principal component analysis (PCA) yielded a clear separation of slow-1 fibers from the fast-types along component one. Fast-2A and 2X showed some overlap. Interestingly, fibers assigned as mixed type distributed between the pure groups expected by their MYH composition (Figure 1C). The PCA loadings indicate that many mitochondrial proteins and slow muscle protein variants, such as the ER calcium ATPase ATP2A2, drive the separation of slow from fast fibers. The latter express typical fast contractile proteins and the ATP1A1 isoform (Figure 1D). Unsupervised hierarchical clustering on the proteins with significantly different expression between at least two of the three fiber types (ANOVA) yielded a vertical separation into fiber types (with only three exceptions, see arrows). In addition, it showed clusters with significant annotation enrichments in fast structural proteins (myosin II complex) and proteins involved in glycogen metabolism limited to fast 2A and 2X fibers. Conversely, slow contractile proteins (termed cardiac, as many slow muscle isoforms are also expressed in cardiac muscles) as well as mitochondrial protein were enriched in slow-1 fibers (Figure S1F). The latter cluster is shared with fast-2A fibers as expected from the rather high mitochondrial content characterizing this fiber type in humans (33).

Pearson's correlation coefficients of all single fibers per individual (median expression), ranged from 0.82 to 0.90 for the least to the most similar subjects. For fiber types, the average Pearson's correlation between slow-1 and fast-2X fibers was 0.79 and was thus lower than the correlation among different donors (average 0.86). Thus, at the proteome level, differences among fiber types outweigh those between subjects. The two astronauts had comparably low Pearson correlation, indicating high variability and different activity load between the two subjects (Figure S1G) (5). Our proteomic quantification of muscle fibers and whole muscle lysates resulted in over 95% coverage of specific structural features of the skeletal muscle such as contractile proteins and sarcoplasmic reticulum as well as over 90% of broader annotations such as respiratory chain, ribosome and proteasome (Figure S1H).

### **Costameric proteins are prominently regulated by bed rest-induced unloading in muscle fibers**

We carried out ANOVA comparing the proteomes of single fibers isolated at BR0, BR5 and BR10, to retrieve the proteins with significantly different expression ( $p < 0.05$ ) between at least two time points (Table S7). After excluding typical plasma protein annotations (likely the result of blood traces and co-isolation of segments of blood capillaries on fiber surface), proteins down-regulated during bed rest were uniquely enriched in pathways of cell adhesion and interaction with the extracellular matrix. This finding indicates that the tight interaction of fibers and matrix, a fundamental relay between fiber contraction and movement, are actively maintained by weight loading and decrease in its absence. Categories "actomyosin", "Z disk" and "calcium channel" were also significantly decreased during bed rest, suggesting that loss of muscle mass measured during bed rest is accompanied by remodeling at the level of sarcomeres and excitation-contraction coupling (Figure S2A).

Force transmission in muscle fibers is based on the structural connection between sarcomeres and the extracellular matrix and mediated by several protein complexes. The two main anchoring structures involved in force transmission are the myotendinous junction (MTJ) and costameres (34). The former connects each fiber to a segment of the tendon, the latter harbors a multitude of functionally cooperating protein complexes connecting the Z disk of the sarcomere to the sarcolemma and further to matrix proteins (schematically represented in Figure 2A). From BR0 to BR10 we observed a decrease in the median expression of several components of the dystroglycan complex (DGC), the main transmembrane anchoring

structure of the costameres connected to dystrophin on the cytosolic side (35) (Figure S2B). The expression of key proteins involved in fiber-matrix adhesion, associated both with costameres and with the MTJ, was also significantly downregulated during bed rest (Figure 2B). In total, based on summed expression, costamere and MTJ protein abundance decreased 20% over 10 days of unloading (Figure 2B above x axis). We ranked the expression of the most significantly regulated proteins, namely Xin actin-binding repeat-containing protein 1 and 2 (XIRP1, XIRP2) and utrophin (UTN), at each BR time in a heat map (BR0, N=78, BR5, N=75, BR10 N=80). We observed a progressive shift towards lower intensities from BR0 to BR10, indicating that more fibers expressed these proteins at lower levels in the unloading phase (Figure 2C). Plakoglobin/gamma catenin (JUP) is a component of desmosomes and adherens junctions, interacting with desmoglein (DSG1) and desmoplakin (DSP) in many cell types. In skeletal muscle, JUP is the key component of a newly discovered sarcolemmal signaling complex interacting with the dystroglycan complex (DGC) at the costameres (36, 37). We observed a consistent decrease in the expression of several members of this complex in response to bed rest. The summed intensity of the complex was reduced by 25% after 10 days of unloading (Figure 2D). JUP, DSP and DSG1 also showed highly significant decreases during bed rest, as an effect of many individual fibers shifting towards lower expression over time (Figure 2E).

We validated the downregulation of the complexes involved in fiber-matrix interaction and force transmission by immunofluorescence with antibodies specific for XIRP2 and JUP on cross sections of muscle biopsies of all ten volunteers involved in the study. (Figure 2F). Comparing section of biopsies from BR0 with those of BR10 by quantitative image analysis, confirmed a significant decrease ( $p < 0.05$ ) in the expression of XIRP2. JUP expression tended to decrease, but the variability among donors was higher (Figure 2G). XIRP1 also showed a significant downregulation comparing BR0 and BR10 (Figure S2C-D).

The proteins whose expression increased during bed rest were most significantly enriched in annotations related to protein turnover (proteasome, elongation factor, chaperone, hypusine), anti-oxidant and stress response as well as carbohydrate metabolism, the latter comprised in the term "glycolysis" (Figure S2E). Indeed, the enzymes involved in the core reactions of glycolysis increased in abundance during bed rest (Figure 2H-I), similarly to proteasomal proteins (Figure 2J-K) and anti-oxidant enzymes (Figure 2L-M). Translation initiation and elongation factors were also enriched among the proteins increasing their expression at BR10 compared to BR0, though the trend was variable for different members of this functional group (Figure S2F-G). Interestingly, the translation initiation/elongation factor EIF5A, the only mammalian protein containing the modified amino acid hypusine (38) was significantly upregulated during bed rest, as indicated by the over 70-fold enrichment in this annotation (see Figure S2E). In addition, we found that the enzymes specifically catalyzing EIF5A hypusination at amino acid residue lys50, deoxyhypusine synthetase (DOHS) and deoxyhypusine hydroxylase (DOHH) were also concomitantly upregulated upon unloading (Figure S2H).

### **Fiber type-specific and fiber type independent proteomic changes induced by bed rest**

Proteomic studies have shown that slow and fast fiber types undergo different changes in response to training (26) and during aging (27, 39). To explore the effects of unloading on the proteome of individual fiber types, we carried out ANOVA between the three times of bed rest comparing only the pure fibers of each type. We then retrieved the proteins that were significantly up- and down-regulated in the course of bed rest in each fiber type.

Fiber types displayed unique sets of proteins significantly regulated during bed rest, with only two proteins commonly downregulated and none commonly upregulated in all three fiber types (Figure 3A). The former two were the Z disk protein Nebulin-related-anchoring protein (NRAP) and XIRP2 whose expression ratio BR10/BR0 decreased more for the fast fiber types 2A and 2X. (Figure 3B and Table S8). We then visualized the expression ratio BR10/BR0 of

the most significantly downregulated proteins ( $p < 0.01$ ) in slow-1, fast-2A and fast-2X fiber types respectively (Figure 3C and Table S8). We observed that proteins upregulated at BR10 in slow-1 fibers were uniquely enriched in annotations related to ROS detoxification and carbohydrate metabolism (Figure 3C and S3A). Indeed, peroxiredoxin 1 (PRDX1) and glyceraldehyde 3-phosphate dehydrogenase (GAPDH) were upregulated only in slow-1 fibers during bed rest (Figure 3D), together with other ROS detoxifying enzymes (Figure S3B). Some proteasomal subunits, like PSMA3 and 7, which showed increased expression in slow-1 and fast-2A but not in fast-2X fibers (Figure S3C).

We asked whether the observed fiber type-specific increase in detoxifying enzymes could reflect fiber type-specific changes in expression or composition of the five respiratory chain complexes, which are the main source of ROS. To this end we calculated the median expression of each complex (schematically represented in Figure S3D) in muscle fibers of the same type at the three BR time points and detected small-sized expression changes comparing fibers isolated pre-bed rest with those isolated after 5 and 10 days of unloading. All five complexes showed a transient increase at BR5 in slow-1 fibers, which reverted to pre-bed rest levels at BR10. (Figure S3D). The subtle but consistent changes in the expression of RC complexes might be linked to variations in shape and connection of the mitochondrial network, which accompanies muscle plasticity and takes part in the regulation of muscle mass (40, 41). We analyzed the expression of main players of mitochondrial fission and fusion, which regulate the architecture of the mitochondrial network. Three proteins involved in mitochondrial fusion (OPA1, MFN1 and MFN2) and the protease AFG3L2 showed significantly lower expression ( $p < 0.05$ ) in muscle fibers at BR10 compared with BR0. Conversely, the expression of BAX, a proapoptotic protein which associates with the outer membrane when mitochondria undergo fission, increased significantly at BR10 (Figure 3E). These and other proteins controlling the architecture of the mitochondrial network had fiber type-specific expression changes in response to unloading (Figure 3F). This might be linked to a different response to atrophy-inducing signals of slow and fast fibers observed in various pathophysiological conditions (42).

As mentioned above, loss of muscle mass measured during bed rest in this cohort (9) is accompanied by remodeling at the level of sarcomeres and excitation-contraction coupling (see Figure S2). As sarcomeric and EC coupling proteins are highly fiber type-specific, we calculated their median expression in all pure and mixed fiber types separately. We then calculated the fold change over BR0 of the median expression of all single fibers isolated at BR5 and BR10. We observed few significant changes for myosins, possibly due to their long half-life (43) and troponins as well as for intermediate filaments and associated proteins and the Z disk (Figure S3E-I). Comparably more proteins of the sarcoplasmic reticulum and T-tubule involved in EC coupling had significant expression changes during bed rest (Figure S3J), suggesting that unloading is associated with structural rearrangements of the SR, which might contribute to the decreased performance measured at whole muscle level in this bed rest cohort (9).

### **Signatures of muscle unloading from spaceflight and bed rest.**

Spaceflight poses complex challenges to the human body which are only partially reproducible at Earth gravity. We asked which proteomic changes of muscle fibers during unloading on Earth could recapitulate the behavior of muscle in microgravity. To this aim, we quantified over 7000 proteins from whole muscle lysates of two crew members of a 6 months ISS mission. We measured technical quintuplicates of muscle biopsies taken 75 days before flight (Pre), one day after landing (La+0) and during muscle recovery after 14 days of reloading on Earth (La+14). MYH composition measured by MS in the soleus biopsies showed a large majority of slow fibers expressing MYH7, with minor fluctuations at the three phases of the mission (Figure S4A). This indicates negligible fiber type changes, possibly due to the intensive training which was adopted as a countermeasure on the ISS. We then carried out ANOVA separately for each astronaut and performed subsequent analyses

only on proteins that changed in expression significantly and with the same trend in both astronauts (Table S9). Based on the expression ratio over the day of landing, we observed that the proteins with significant expression changes had an opposite expression trend between the mission phases, following the switch of loading conditions. This indicates that the expression of these proteins is directly or indirectly regulated by weight load, either negatively (Figure 4A) or positively (Figure 4B).

Within the proteins significantly up-regulated after spaceflight and down-regulated during re-loading on Earth we observed enrichments in annotations of the extracellular matrix, including collagens and laminin (Figure 4C) suggesting a link between muscle loading and the control of matrix composition (44). It is possible that muscle fiber atrophy changes the ratio between contractile tissue and extracellular matrix without changing the absolute amount of connective tissue, as shown recently in a study of 60 days bed rest (45). The relative increase in matrix components measured by MS in the biopsies post-flight likely correlates with structural remodeling. Indeed, extensive changes in muscle morphology correlating with atrophy were previously shown in these two astronauts using transversal magnetic resonance and ultrasonography (5). The proteins positively regulated by weight load were specifically enriched in mitochondrial annotations related to energy metabolism (Figure 4D).

We thus compared the mitochondrial proteome of astronauts at different times of the mission under different loading conditions. Over 90% of mitochondrial proteins (225 of 238 significant) were expressed at significantly lower levels post-mission than on the day of landing, corresponding to a 35% loss of total mitochondrial protein intensity (Figure 4E, S4B). This effect was prominent for the components of the respiratory chain (48 of 71, black dots in Figure 4E, Table S10). This was partially reversed after re-loading at Earth gravity (Figure 4F, S4C). Interestingly, only 50 % of the subunits encoded by mitochondrial DNA (4 of 8, red dots) showed significant downregulation in spaceflight, a finding that is also validated by a previous report (17). The expression of eighteen respiratory chain components was higher 14 days after landing than it was before the flight (Figure 4G). After two weeks at Earth gravity, 25% of the respiratory chain protein intensity lost at R+0 had been recovered (Figure S4C).

Three proteins were significantly downregulated during unloading both in bed rest and in the two astronauts in spaceflight, namely fatty acid-binding protein 5 (FABP5), calcineurin B homologous protein (CHP1) and DSG1 (Figure 4H). Six proteins that decreased their expression during bed rest were upregulated in astronauts after 14 days of re-loading on Earth, two of which were those downregulated during spaceflight (Figure 4H-I, labelled in red). DSG1 and DSP are physical interactors and part of a functional complex with JUP, which is also significantly upregulated upon muscle re-loading in astronauts (Figure 4I and see Figure 3). Our results thus show that the expression of focal adhesion proteins at the costameres is promoted and/or maintained by weightbearing muscle activity. JUP and its associated proteins have been shown to stabilize the insulin receptors on the sarcolemma (37). The amount of membrane insulin receptor in muscle was shown to be rate-limiting for insulin signaling (46). This suggests the possibility of a link between insulin resistance, which affects astronauts during space flights (47) and was measured in our study subjects undergoing bed rest (see Table S1), and the decrease of JUP and associated proteins occurring in muscle unloading.

Twenty-seven proteins were significantly upregulated during both spaceflight and bed rest, indicating that their expression in skeletal muscle increases under muscle unloading and disuse (Figure S4D). They were specifically enriched in nucleotide biosynthesis and redox annotations (Figure S4E).

We previously showed that ten days of bed rest caused neuromuscular junction (NMJ) damage, as indicated by the upregulation of neural cell adhesion molecule 1 (NCAM1) and other markers of NMJ damage and proposed that NMJ damage underlies the greater decline in muscle force than in muscle size which is typically measured after muscle unloading (9). Interestingly, we here observed that NCAM1 expression was significantly increased in the

biopsies of astronauts sampled on the day of landing and remained higher after two weeks on Earth (Figure S4F).

## Discussion

In spaceflight, atrophy is more prominent in slow-1 than in fast fibers and typically affects postural muscles such as soleus (8). Thus, a fiber type-resolved omics approach to inactivity would be instrumental for further clarifying the molecular basis of muscle dysfunction affecting astronauts. Here we measured the proteome of single muscle fibers from subjects in bed rest to discover fiber type-specific changes which could not be extricated in a whole muscle lysate. We then measured the muscle lysate of astronauts after a mission on the ISS with the same proteomic platform and workflow. From the integration of the two datasets, it is possible to mine the contribution of specific fiber types to the phenotype of unloaded muscle.

Previous transcriptome and proteome analyses of skeletal muscle during bed rest have shown downregulation of mRNAs annotated to cell adhesion and cytoskeleton (21, 48) and assessed the effects of countermeasures (49, 50). We specifically uncovered a rapid and progressive downregulation of costameric structures, corresponding to the focal adhesions of skeletal muscle, in agreement with previous observations in a model of tendon release in sheep (51). The costameres also accommodate a recently identified signaling hub containing desmosomal components, including plakoglobin (JUP) and the insulin receptor, which activates the PI3K-FOXO signaling preventing muscle atrophy (36). We have measured a significant decrease in the expression of JUP, desmoglein (DSG1) and desmoplakin (DSP), as well as other interactors of this molecular complex (37) in bed rest. The same proteins were also downregulated after spaceflight in astronauts and their expression was significantly upregulated after 14 days of normal locomotor activity on Earth (schematically represented in Figure 5).

Compared to the changes observed in transcriptome studies of bed rest, particularly at longer time points, the proteomic changes we measure here are generally smaller in size and limited to a lower number of significant hits (52). Long protein half-lives of contractile proteins (53) may account for part of this difference, as we could detect changes in MYH transcripts in the muscle lysate of these subjects in a previous study (9) which we did not measure here at the proteome level. Interestingly however, the mitochondrial protein changes in astronauts showed an overlapping with the regulated transcripts reported after long spaceflights (17, 19).

Muscle inactivity and unloading are linked to glucose intolerance (54) and both astronauts and bedridden subjects consistently display alterations in insulin sensitivity (47). We propose that JUP and its associated membrane complex, through their stabilizing action on insulin receptors, play a key role in preserving insulin sensitivity under muscle loading conditions. In addition, we detected downregulation of several members of the sarcoglycan complex and the Xin repeat-containing proteins and utrophin, located both at the costameres and at the myotendinous junction. Our fiber type-resolved analysis showed that the unloading time-dependent downregulation was generally larger in fast than in slow fibers. In addition, fast fibers tended to have higher basal expression of costameric proteins and thus contributed most to the bulk downregulation of these adhesion structures. The myotendinous junction is responsible for the tight association between muscle fibers, directly or through the aponeurosis, and the connective tissue of the tendon and thus relays the contractile force generated in the sarcomere to the locomotor apparatus. In the same cohort of voluntary bed rest, we have previously shown that knee-extensor isometric maximum voluntary contraction decreased by more than 14% in ten days, while the mid-muscle cross sectional area of vastus lateralis was reduced by 5.8% (9). We detected damage to the neuromuscular junction and proposed that this degenerative process induced by unloading underlies the decrease in muscle force exceeding the loss of muscle mass (9). Here, we measured over 10-fold increase in neural cell adhesion molecule (NCAM), a marker of muscle denervation, in the muscle biopsies of astronauts on the day of landing compared to pre-flight. This confirms that



impaired muscle nerve connection also occurs under microgravity condition and might contribute to the drastic loss of muscle force in astronauts after landing. In addition, we hypothesize that the significant decrease in protein complexes responsible for lateral and longitudinal force transmission, combined with matrix remodeling, could be a further muscle-intrinsic change whereby mechanical unloading causes a decrease in whole muscle contractile force.

The initiation/elongation factor EIF5A was one of several proteins involved in translation which we found significantly upregulated during bed rest. The expression of translational regulators has recently been shown to not follow the lower translation rate underlying the onset of atrophy in immobilized mouse muscles (55). Active EIF5A contains an unusual spermidine-derived amino acid residue at position 50, hypusine, which is unique in the human proteome and essential for the translational elongation activity. We show that the two enzymes responsible for EIF5A hypusination, deoxyhypusine synthase and deoxyhypusine hydroxylase, are also upregulated during bed rest (see Figure S2). EIF5A promotes the expression of OXPHOS and TCA proteins in macrophages (56) and its upregulation in unloaded muscle could thus be a compensatory mechanism to preserve oxidative capacity. Alternatively, hypusinated EIF5A might be inducing autophagy, through its ability to regulate the synthesis of transcription factor EB (TFEB) a master regulator of this pathway (57). Further definition of the role of EIF5A in unloading-mediated muscle atrophy might allow to target this unique molecular axis with existing drugs.

Our data show that ten days of bed rest cause a significant decrease in the abundance of the mitochondrial dynamin like GTPase OPA1, of the mitochondrial outer membrane GTPase mitofusin (MFN1 and MFN2) and of the matrix protease AGF3L2. As these proteins are major regulators of mitochondrial fusion-fission/balance (58), muscle unloading might be linked to variation in shape and connection of the mitochondrial network, which have been shown to accompany pathological muscle remodeling. Indeed, loss of OPA1 causes muscle atrophy in mice (41) and muscle-specific knockout of MFN1 and 2 leads to a significant reduction in exercise performance (59). In addition, downregulation of the mitochondrial AAA protease AFG3L2 has been linked to constitutively active mitochondrial calcium uniporter (MCU) caused by the accumulation of the essential MCU regulator (EMRE) leading to neurotoxicity (60). This mechanism may be involved in the NMJ damage that we previously detected in individuals undergoing bed rest (9). It is tempting to speculate that muscle unloading causes rearrangements of the mitochondrial network by changing the expression of its master regulators.

While ten days of bed rest caused subtle changes in the mitochondrial proteome, six-month spaceflight caused a sharp decrease in the expression of the whole mitochondrial proteome, including the respiratory chain, in agreement with previous reports (17, 61). Interestingly, this was not accompanied by major changes in MYH isoforms composition, thus it was not driven by a fiber type shift. As the muscle biopsies of soleus from the two astronauts contained a large majority of slow fibers expressing MYH7 (see Figure S4A), most of the changes in the mitochondrial proteome measure here occurred in slow fibers. The different behavior of the mitochondrial proteome during bed rest and spaceflight might be a simple function of time. However, we observed that spaceflight-induced downregulation of the mitochondrial proteome is effectively reverted after two weeks of normal reambulation on Earth. Thus, strikingly, large loading-dependent changes in the expression of the respiratory chain occur in a timescale of days. It is conceivable that other challenges of spaceflight different from unloading are also causing OXPHOS defects. Amongst these, we cannot exclude the impact of cosmic radiation on most biological processes and tissue, increasing the risk of damage to DNA, the cell membrane, the cardiovascular system, the nervous and lymphatic systems, stem cells (62, 63). Since the astronauts in our cohort were training daily on the ISS, our data also indicate that the cause-effect relationship between low-medium intensity, long duration exercise (performed on the ISS) and mitochondrial biogenesis (12) is fundamentally altered under microgravity conditions.

In conclusion, our experimental design based on the MS analysis of individual fibers provided single cell-resolved data on muscle-intrinsic proteome changes devoid of the contribution of other cell types which are found in whole lysate. This feature of the dataset was instrumental to show that plakoglobin and its associated proteins (also expressed in endothelium and blood cells) decreased significantly after spaceflight in the muscle of astronauts. In addition, we could highlight that only slow-1 fibers significantly upregulated peroxiredoxins and superoxide dismutase, an indication that their antioxidant defense is stronger than that of fast fibers. Microgravity-induced loss of muscle strength is greater than the corresponding loss of muscle mass and largely exercise-resistant. Mechanistically, genetic tools that are protective against muscle atrophy on Earth, such as the knockout of the ubiquitin ligase MuRF1 do not rescue muscle mass under microgravity conditions (64). As muscle atrophy leads to spiraling adverse effects for the organism, addressing this conundrum will be crucial for manned missions in deep space.

## Materials and Methods

### Patient cohorts and samples

For the bed rest cohort, single fibers were dissected from muscle biopsies of ten healthy volunteers (Table S1) previously characterized and analyzed (9). Experiments were carried out with approval from the National Ethical Committee of the Slovenian Ministry of Health, with the reference number 0120-304/2019/9 and complied with the guidelines of the 2013 Declaration of Helsinki. The subjects spent 15 consecutive days at the Izola General Hospital (Izola, Slovenia). The protocol included 3 days of familiarization to the study environment and diet. Muscle biopsies were carried out on vastus lateralis muscle pre-bed rest (BR0, right leg), after 5 days of bed rest (BR5, left leg) and after 10 days of bed rest (BR10, right leg). For the astronaut cohort, two crew members of equal sex and comparable age, were enrolled in the Sarcolab study (5) and tested before and after their half-year mission on the International Space Station. All procedures were performed in accordance with the guidelines and approved by the Committee for the Protection of Human Subjects (NASA MPA number 7116301606HR, Protocol number 09-3940-Ren-2-Air-1). Muscle biopsies were obtained pre-flight (day -79 and -76 for the two subjects respectively), on the day of landing (R+0) and 14 days after landing (R+14). Written informed consent was obtained from all subjects prior to study inclusion.

### Single fibers sample processing

Fibers were microdissected manually under a stereomicroscope from fresh biopsies kept in an ice-cold solution containing K-propionate (150mM), KH<sub>2</sub>PO<sub>4</sub> (5mM), Mg Acetate (5mM), EGTA (5 mM) and DTT (1mM). They were individually frozen in dry ice in standard Eppendorf tubes. The fiber isolation was completed within 20 minutes of the muscle biopsy procedure. Fibers were lysed in 20  $\mu$ l of LYSE (PreOmics), heated at 95°C for 5 min and sonicated in a water-bath sonicator (Diagenode) for 15 min. with a 50% duty cycle. Proteolytic digestion was carried out by adding to the fiber lysate 500 ng of endoproteinase LysC and 500 ng of trypsin in 10  $\mu$ l of LYSE buffer. After overnight digestion at 37°C under continuous shaking, the lysate was acidified to a final concentration of 0.1% trifluoro-acetic acid (TFA) and loaded onto StageTip plugs of SDB-RPS. Purified peptides were eluted with 80% acetonitrile-1% ammonia and dried. The dataset consists of 233 single fibers, obtained from 10 subjects at 3 time points.

### Total muscle lysate sample processing

Muscle lysates of astronauts in RIPA buffer were precipitated in acetone and resuspended in LYSE buffer (PreOmics), heated at 95°C for 5 min and sonicated in a water-bath sonicator

(Diagenode) for 15 min. with a 50% duty cycle. Protein concentration in the lysate was adjusted to 2 µg/µl. Proteolytic digestion was carried out by adding 1 µg of endoproteinase LysC and trypsin per 50 µg of lysate. After overnight digestion at 37°C under continuous shaking, the lysate was acidified to a final concentration of 0.1% trifluoro-acetic acid (TFA) and loaded onto StageTip plugs of SDB-RPS. Purified peptides were eluted with 80% acetonitrile-1% ammonia and dried. The dataset consists of technical quintuplicates for the biopsies of 2 astronauts at 3 time points.

### **Library generation**

We generated two peptide libraries, from whole muscle homogenate and human cultured myoblasts and used the MaxQuant match between run function (Figure 1). To prepare the human muscle library, a fragment of 5 mg of vastus lateralis was crushed in liquid nitrogen and resuspended in 200 µl of LYSE. Human myoblasts were dissolved in LYSE. Both lysates were heated at 95°C for 5 min and sonicated in the water-bath sonicator for 15 min. After measuring protein concentration, 100 µg of each lysate were digested in a total volume of 200 µl of LYSE 5 µg of endoproteinase LysC for at 25°C for 3 hs under continuous stirring. The sample was further sonicated and 5 µg of trypsin were added, followed by overnight incubation at 37°C. Peptides were desalted on StageTip plugs of SDB-RPS and eluted into 16 fractions using a Spider Fractionator (65).

### **Liquid chromatography and mass spectrometry.**

Peptides were separated on 50 cm columns of ReproSil-Pur C18-AQ 1.9 µm resin (Dr. Maisch GmbH) packed in-house. The columns were kept at 60 °C using a column oven. Liquid chromatography-mass spectrometry (LC-MS) analysis was carried out on an anEASY-nLC-1200 system (Thermo Fisher Scientific) connected to a trapped ion mobility spectrometry quadrupole time-of-flight mass spectrometer (timsTOF Pro, Bruker Daltonik) (Meier et al., 2018). A linear 60 min gradient from 5-30% B in 47.5 min was applied, followed by an increase to 60% for 2.5 min, by a 5 min wash at 95% buffer B at 300nl/min and reequilibration for 5 min at 5% buffer B (Buffer A: 0.1% Formic Acid; Buffer B: 0.1% Formic Acid, 80% acetonitrile). For ddaPASEF, 1 MS1 survey TIMS-MS and 10 PASEF MS/MS scans were acquired per acquisition cycle. Singly charged precursor ions were excluded with a polygon filter (otof control, Bruker Daltonik GmbH). A dynamic exclusion of 40 s elution was applied.

### **Immunofluorescence of muscle sections and image analysis**

Muscle biopsies were cut into 10 µm thick cryosections and fixed with 4% PFA for 15 min at RT, then heated in sodium citrate buffer, pH 6.0, at sub-boiling temperature for 40 minutes in microwave oven (550W). Sections were then stained with anti-XIRP1 (1:500, HPA016750, rabbit polyclonal IgG, Atlas Antibodies), or anti-XIRP2 (1:50, HPA034813, rabbit polyclonal IgG, Atlas Antibodies), or anti-JUP (1:50, AP33204SU-N, guinea pig polyclonal antibody, Origene) and co-stained with anti-dystrophin (1:100, MANDRA1 (7A10), mouse monoclonal, DSHB, Iowa University), in PBS with 1% BSA overnight at 4°C. The sections were stained with Hoechst prior to mounting with a saturated solution of polyvinyl alcohol with 30% glycerol.

16-bit gray scale raw images were acquired with a Leica DM6B microscope, equipped with a DFC 7000T camera, and quantified with FIJI (ImageJ v. 1.53c, NIH). Muscle sections were manually outlined with freehand selection tool and mean gray value for each muscle was measured. Mean gray value was also recorded in regions adjacent to the muscle section, and used to get background-subtracted values, to normalize for possible differences between sections and slides.

## Plasma glucose and insulin measurement

The concentration of insulin was measured in plasma by double-antibody immunoassay, the concentration of glucose by use of the hexokinase reaction. Measurements were carried out on Cobas c502 and e801 automated clinical chemistry analyzers respectively (Roche Diagnostics GmbH). The estimate of insulin resistance by HOMA-IR was calculated with the formula fasting serum insulin ( $\mu\text{U/ml}$ ) $\times$  fasting plasma glucose ( $\text{mmol/l}$ )/22.5, as described (66).

## Computational proteomics

The MaxQuant software (version 1.6.15.0) was used for the analysis of raw files searching against the human Uniprot databases (UP000005640\_9606, UP000005640\_9606\_additional) and a common contaminants database (67). The FDR was set to 1% for peptides (minimum length of 7 amino acids) and proteins and was determined by searching a reverse database. Peptide identifications by MS/MS were transferred by matching between the runs with a 0.7-min retention-time match window between single fibers, the two libraries and 5 technical replicates of total lysate before fractionation. Peptides with a minimum length of seven amino acids were considered for the search including N-terminal acetylation and methionine oxidation as variable modifications and cysteine carbamidomethylation as fixed modification. Enzyme specificity was set to trypsin cleaving c-terminal to arginine and lysine. A maximum of two missed cleavages was allowed. For MYH isoforms specifically, only peptides unique to each isoform were used for quantification in MaxQuant.

## Bioinformatic and statistical analysis

All analyses were performed with the Perseus software (version 1.6.14.0), part of the MaxQuant environment (68). Label free quantification values were used throughout the analysis for protein expression, using the feature implemented in MaxQuant (67). ANOVA was performed using 0.05 FDR for truncation and 250 randomizations unless otherwise specified. Tukey's Honest Significant Difference procedure was used as post-hoc test. Unequal variance was assumed between the groups and Welch t-test was used for two samples comparisons with  $p < 0.05$  as a threshold. Categorical annotations were supplied in the form of UniProt Keywords, Corum, KEGG and Gene Ontology. Annotation enrichments were calculated by Fisher exact test using 0.02 Benjamini-Hochberg FDR for truncation and the Uniprot human proteome as background. Individual fibers were treated as individual samples (biological replicates) and statistics did not take the subjects of origin into account (based on Pearson correlation in figure S1 and see (27)). For figures 3 and 4, protein expression in different fiber types was converted into circles relative to the expression in type 1 fibers set at a fixed diameter. For the single fibers dataset, n was as follows: (i) time. BR0, n= 78; BR5, n=75; BR10, N=80. (ii) fiber type. 1-slow, n=82; fast-2A, n=56; fast-2X, n=25; mixed1/2A, n=17; mixed2A/2X, n=53. For the astronaut dataset, each biopsy was measured in technical quintuplicates. ANOVA was performed separately for each astronaut and the lists of significant proteins ( $p < 0.05$ ) were crossed for common hits only. For graphs with column scatter, n=10 at three time points.

## Fiber type assignment

We used the proteomic quantification of four adult myosin heavy chain (MYH) isoforms to assign fiber type by MS analysis. Since different isoforms of MYH have more than 80% sequence identity; we based our quantification on the intensities of peptides unique for each isoform (69, 70). We summed the intensities of MYH7 (slow-type 1), MYH2 (fast-2A), MYH1 (fast-2X) and MYH4 (Fast-2B) and calculated for each fiber their respective amount in

percent. We initially split the fibers into three groups according to the majority isoform they expressed. We then calculated the median expression of the majority MYH isoform as a proxy for purity, which was 98% for MYH7/slow-1 and 78% for both MYH2/fast 2A and MYH1/fast-X (MYH4 is present only in trace amounts in humans). Approximating to lower 10%, we set a threshold of 90% for MYH7 and 70% for MYH1 and MYH2.

### Acknowledgments

We are grateful to I. Paron, and A. Piras for their assistance with MS; Thomas Klopstock (LMU Muenchen) for the human myoblasts, Lorenza Brocca (University of Pavia), Leonardo Nogara and Elena Monti (University of Padova) and Mariella Sturma (University of Trieste) for their precious help with sample collection and fiber isolation, Mladen Gasparini (Izola General Hospital) for performing the biopsies, the bed rest team and Izola General Hospital personnel and to the volunteers enrolled this study. We thank Joern Rittweger (German Aerospace Center, Cologne, Germany) for the muscle lysates of the Sarcolab project. We are grateful to Henning Wackerhage (Technical University, Munich Germany), Kenneth Dyar (Helmholtz Zentrum, Munich, Germany), Katrien De Bock (ETH, Zurich, Switzerland) and Markus Ruegg (Biozentrum, Basel CH) for their critical analysis of the manuscript.

### Data availability

All study data are included in the article, SI Appendix, and Datasets S2 to S10. The mass spectrometry proteomics data have been deposited to the ProteomeXchange Consortium via the PRIDE partner repository with the dataset identifier PXD028435.

### References

1. S. Schiaffino, C. Reggiani, Fiber types in mammalian skeletal muscles. *Physiol Rev* **91**, 1447-1531 (2011).
2. S. P. Kilroe *et al.*, Dietary protein intake does not modulate daily myofibrillar protein synthesis rates or loss of muscle mass and function during short-term immobilization in young men: a randomized controlled trial. *Am J Clin Nutr* **113**, 548-561 (2021).
3. T. A. Trappe, N. A. Burd, E. S. Louis, G. A. Lee, S. W. Trappe, Influence of concurrent exercise or nutrition countermeasures on thigh and calf muscle size and function during 60 days of bed rest in women. *Acta Physiol (Oxf)* **191**, 147-159 (2007).
4. M. D. de Boer, C. N. Maganaris, O. R. Seynnes, M. J. Rennie, M. V. Narici, Time course of muscular, neural and tendinous adaptations to 23 day unilateral lower-limb suspension in young men. *The Journal of physiology* **583**, 1079-1091 (2007).
5. J. Rittweger *et al.*, Sarcolab pilot study into skeletal muscle's adaptation to long-term spaceflight. *NPJ Microgravity* **4**, 18 (2018).
6. R. Demangel *et al.*, Early structural and functional signature of 3-day human skeletal muscle disuse using the dry immersion model. *J Physiol* **595**, 4301-4315 (2017).
7. L. Brocca *et al.*, FoxO-dependent atrogenes vary among catabolic conditions and play a key role in muscle atrophy induced by hindlimb suspension. *The Journal of physiology* **595**, 1143-1158 (2017).
8. R. H. Fitts *et al.*, Prolonged space flight-induced alterations in the structure and function of human skeletal muscle fibres. *J Physiol* **588**, 3567-3592 (2010).
9. E. Monti *et al.*, Neuromuscular junction instability and altered intracellular calcium handling as early determinants of force loss during unloading in humans. *J Physiol* 10.1113/JP281365 (2021).
10. T. Trappe, Influence of aging and long-term unloading on the structure and function of human skeletal muscle. *Appl Physiol Nutr Metab* **34**, 459-464 (2009).
11. M. L. Dirks *et al.*, One Week of Bed Rest Leads to Substantial Muscle Atrophy and Induces Whole-Body Insulin Resistance in the Absence of Skeletal Muscle Lipid Accumulation. *Diabetes* **65**, 2862-2875 (2016).
12. J. M. Memme, M. Slavin, N. Moradi, D. A. Hood, Mitochondrial Bioenergetics and Turnover during Chronic Muscle Disuse. *Int J Mol Sci* **22** (2021).

13. J. A. Hawley, M. Hargreaves, M. J. Joyner, J. R. Zierath, Integrative biology of exercise. *Cell* **159**, 738-749 (2014).
14. K. L. English *et al.*, High intensity training during spaceflight: results from the NASA Sprint Study. *NPJ Microgravity* **6**, 21 (2020).
15. N. Petersen *et al.*, Exercise in space: the European Space Agency approach to in-flight exercise countermeasures for long-duration missions on ISS. *Extrem Physiol Med* **5**, 9 (2016).
16. E. Afshinnekoo *et al.*, Fundamental Biological Features of Spaceflight: Advancing the Field to Enable Deep-Space Exploration. *Cell* **183**, 1162-1184 (2020).
17. W. A. da Silveira *et al.*, Comprehensive Multi-omics Analysis Reveals Mitochondrial Stress as a Central Biological Hub for Spaceflight Impact. *Cell* **183**, 1185-1201 e1120 (2020).
18. R. H. Fitts *et al.*, Effects of prolonged space flight on human skeletal muscle enzyme and substrate profiles. *J Appl Physiol (1985)* **115**, 667-679 (2013).
19. F. E. Garrett-Bakelman *et al.*, The NASA Twins Study: A multidimensional analysis of a year-long human spaceflight. *Science* **364** (2019).
20. Z. S. Patel *et al.*, Red risks for a journey to the red planet: The highest priority human health risks for a mission to Mars. *NPJ Microgravity* **6**, 33 (2020).
21. Z. S. Mahmassani *et al.*, Age-dependent skeletal muscle transcriptome response to bed rest-induced atrophy. *J Appl Physiol (1985)* **126**, 894-902 (2019).
22. K. Nay *et al.*, Simulated microgravity disturbs iron metabolism and distribution in humans: Lessons from dry immersion, an innovative ground-based human model. *FASEB J* **34**, 14920-14929 (2020).
23. X. Hong *et al.*, Effects of spaceflight aboard the International Space Station on mouse estrous cycle and ovarian gene expression. *NPJ Microgravity* **7**, 11 (2021).
24. C. S. Thiel *et al.*, Rapid coupling between gravitational forces and the transcriptome in human myelomonocytic U937 cells. *Sci Rep* **8**, 13267 (2018).
25. A. S. Deshmukh *et al.*, Deep proteomics of mouse skeletal muscle enables quantitation of protein isoforms, metabolic pathways, and transcription factors. *Mol Cell Proteomics* **14**, 841-853 (2015).
26. A. S. Deshmukh *et al.*, Deep muscle-proteomic analysis of freeze-dried human muscle biopsies reveals fiber type-specific adaptations to exercise training. *Nat Commun* **12**, 304 (2021).
27. M. Murgia *et al.*, Single Muscle Fiber Proteomics Reveals Fiber-Type-Specific Features of Human Muscle Aging. *Cell Rep* **19**, 2396-2409 (2017).
28. R. Vettor *et al.*, The origin of intermuscular adipose tissue and its pathophysiological implications. *Am J Physiol Endocrinol Metab* **297**, E987-998 (2009).
29. A. D. Brunner *et al.*, Ultra-high sensitivity mass spectrometry quantifies single-cell proteome changes upon perturbation. *Mol Syst Biol* **18**, e10798 (2022).
30. G. R. Clement *et al.*, Challenges to the central nervous system during human spaceflight missions to Mars. *J Neurophysiol* **123**, 2037-2063 (2020).
31. C. Gallo, L. Ridolfi, S. Scarsoglio, Cardiovascular deconditioning during long-term spaceflight through multiscale modeling. *NPJ Microgravity* **6**, 27 (2020).
32. L. Vico, A. Hargens, Skeletal changes during and after spaceflight. *Nat Rev Rheumatol* **14**, 229-245 (2018).
33. S. Schiaffino, C. Reggiani, M. Murgia, Fiber type diversity in skeletal muscle explored by mass spectrometry-based single fiber proteomics. *Histol Histopathol* **35**, 239-246 (2020).
34. C. A. Henderson, C. G. Gomez, S. M. Novak, L. Mi-Mi, C. C. Gregorio, Overview of the Muscle Cytoskeleton. *Compr Physiol* **7**, 891-944 (2017).
35. I. N. Rybakova, J. R. Patel, J. M. Ervasti, The dystrophin complex forms a mechanically strong link between the sarcolemma and costameric actin. *J Cell Biol* **150**, 1209-1214 (2000).
36. S. Cohen, D. Lee, B. Zhai, S. P. Gygi, A. L. Goldberg, Trim32 reduces PI3K-Akt-FoxO signaling in muscle atrophy by promoting plakoglobin-PI3K dissociation. *J Cell Biol* **204**, 747-758 (2014).
37. Y. Eid Mutlak *et al.*, A signaling hub of insulin receptor, dystrophin glycoprotein complex and plakoglobin regulates muscle size. *Nat Commun* **11**, 1381 (2020).

38. M. H. Park, The post-translational synthesis of a polyamine-derived amino acid, hypusine, in the eukaryotic translation initiation factor 5A (eIF5A). *J Biochem* **139**, 161-169 (2006).
39. M. M. Porter, A. A. Vandervoort, J. Lexell, Aging of human muscle: structure, function and adaptability. *Scand J Med Sci Sports* **5**, 129-142 (1995).
40. G. Favaro *et al.*, DRP1-mediated mitochondrial shape controls calcium homeostasis and muscle mass. *Nat Commun* **10**, 2576 (2019).
41. C. Tezze *et al.*, Age-Associated Loss of OPA1 in Muscle Impacts Muscle Mass, Metabolic Homeostasis, Systemic Inflammation, and Epithelial Senescence. *Cell Metab* **25**, 1374-1389 e1376 (2017).
42. F. M. Purves-Smith, N. Sgarioto, R. T. Hepple, Fiber typing in aging muscle. *Exerc Sport Sci Rev* **42**, 45-52 (2014).
43. R. W. Tsika, R. E. Herrick, K. M. Baldwin, Time course adaptations in rat skeletal muscle isomyosins during compensatory growth and regression. *J Appl Physiol* (1985) **63**, 2111-2121 (1987).
44. M. D. Boppart, Z. S. Mahmassani, Integrin signaling: linking mechanical stimulation to skeletal muscle hypertrophy. *Am J Physiol Cell Physiol* **317**, C629-C641 (2019).
45. G. K. Thot *et al.*, Effects of long-term immobilisation on endomysium of the soleus muscle in humans. *Exp Physiol* **106**, 2038-2045 (2021).
46. A. Nagarajan *et al.*, MARCH1 regulates insulin sensitivity by controlling cell surface insulin receptor levels. *Nat Commun* **7**, 12639 (2016).
47. R. L. Hughson *et al.*, Increased postflight carotid artery stiffness and in-flight insulin resistance resulting from 6-mo spaceflight in male and female astronauts. *Am J Physiol Heart Circ Physiol* **310**, H628-638 (2016).
48. L. Brocca *et al.*, The time course of the adaptations of human muscle proteome to bed rest and the underlying mechanisms. *J Physiol* **590**, 5211-5230 (2012).
49. E. L. Dillon *et al.*, Proteomic investigation of human skeletal muscle before and after 70 days of head down bed rest with or without exercise and testosterone countermeasures. *PLoS One* **14**, e0217690 (2019).
50. M. Moriggi *et al.*, Long term bed rest with and without vibration exercise countermeasures: effects on human muscle protein dysregulation. *Proteomics* **10**, 3756-3774 (2010).
51. M. Fluck *et al.*, Down-Regulation of Mitochondrial Metabolism after Tendon Release Primes Lipid Accumulation in Rotator Cuff Muscle. *Am J Pathol* **190**, 1513-1529 (2020).
52. R. Fernandez-Gonzalo *et al.*, Three months of bed rest induce a residual transcriptomic signature resilient to resistance exercise countermeasures. *FASEB J* **34**, 7958-7969 (2020).
53. P. Balagopal, O. Ljungqvist, K. S. Nair, Skeletal muscle myosin heavy-chain synthesis rate in healthy humans. *Am J Physiol* **272**, E45-50 (1997).
54. A. C. Alibegovic *et al.*, Insulin resistance induced by physical inactivity is associated with multiple transcriptional changes in skeletal muscle in young men. *Am J Physiol Endocrinol Metab* **299**, E752-763 (2010).
55. K. H. Lin *et al.*, A deep analysis of the proteomic and phosphoproteomic alterations that occur in skeletal muscle after the onset of immobilization. *The Journal of physiology* **599**, 2887-2906 (2021).
56. D. J. Puleston *et al.*, Polyamines and eIF5A Hypusination Modulate Mitochondrial Respiration and Macrophage Activation. *Cell Metab* **30**, 352-363 e358 (2019).
57. H. Zhang *et al.*, Polyamines Control eIF5A Hypusination, TFEB Translation, and Autophagy to Reverse B Cell Senescence. *Mol Cell* **76**, 110-125 e119 (2019).
58. V. Romanello, M. Sandri, The connection between the dynamic remodeling of the mitochondrial network and the regulation of muscle mass. *Cell Mol Life Sci* **78**, 1305-1328 (2021).
59. M. B. Bell, Z. Bush, G. R. McGinnis, G. C. Rowe, Adult skeletal muscle deletion of Mitofusin 1 and 2 impedes exercise performance and training capacity. *J Appl Physiol* (1985) **126**, 341-353 (2019).
60. T. Konig *et al.*, The m-AAA Protease Associated with Neurodegeneration Limits MCU Activity in Mitochondria. *Mol Cell* **64**, 148-162 (2016).
61. H. P. Indo *et al.*, Changes in mitochondrial homeostasis and redox status in astronauts following long stays in space. *Sci Rep* **6**, 39015 (2016).

62. F. A. Cucinotta, Space radiation risks for astronauts on multiple International Space Station missions. *PLoS One* **9**, e96099 (2014).
63. D. K. Fix, J. P. Hardee, T. A. Bateman, J. A. Carson, Effect of irradiation on Akt signaling in atrophying skeletal muscle. *J Appl Physiol* (1985) **121**, 917-924 (2016).
64. S. M. Cadena *et al.*, Skeletal muscle in MuRF1 null mice is not spared in low-gravity conditions, indicating atrophy proceeds by unique mechanisms in space. *Sci Rep* **9**, 9397 (2019).
65. N. A. Kulak, P. E. Geyer, M. Mann, Loss-less Nano-fractionator for High Sensitivity, High Coverage Proteomics. *Mol Cell Proteomics* **16**, 694-705 (2017).
66. D. R. Matthews *et al.*, Homeostasis model assessment: insulin resistance and beta-cell function from fasting plasma glucose and insulin concentrations in man. *Diabetologia* **28**, 412-419 (1985).
67. J. Cox *et al.*, Accurate proteome-wide label-free quantification by delayed normalization and maximal peptide ratio extraction, termed MaxLFQ. *Mol Cell Proteomics* **13**, 2513-2526 (2014).
68. S. Tyanova *et al.*, The Perseus computational platform for comprehensive analysis of (prote)omics data. *Nat Methods* **13**, 731-740 (2016).
69. H. C. Drexler *et al.*, On marathons and Sprints: an integrated quantitative proteomics and transcriptomics analysis of differences between slow and fast muscle fibers. *Mol Cell Proteomics* **11**, M111 010801 (2012).
70. S. Fraterman, U. Zeiger, T. S. Khurana, M. Wilm, N. A. Rubinstein, Quantitative proteomics profiling of sarcomere associated proteins in limb and extraocular muscle allotypes. *Mol Cell Proteomics* **6**, 728-737 (2007).

## Figures and Tables

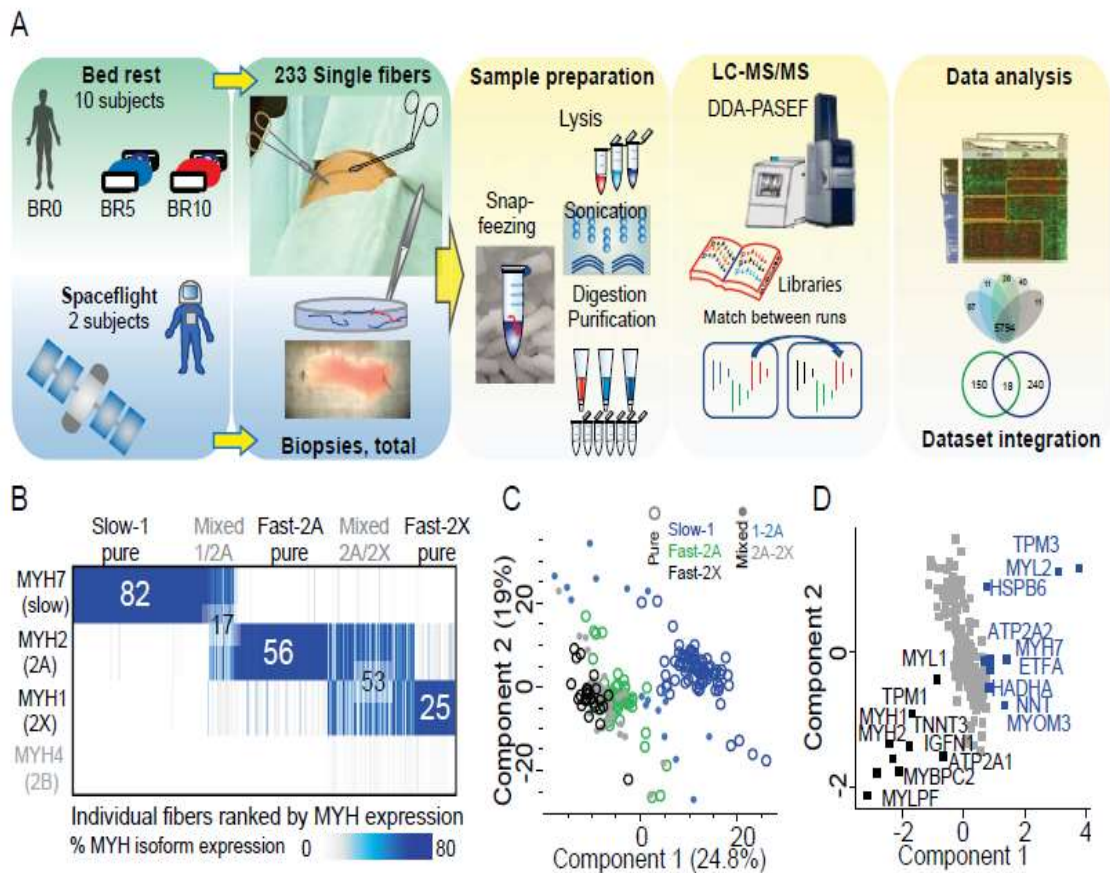


**Figure 1. Proteomic workflow, MS-based muscle fiber type assignment and phenotype.**



**(A)** MS-based proteomics workflow for the preparation and analysis of single muscle fibers from bed rest volunteers, whole lysates from astronauts and samples for library generation. For details see main text and Materials and Methods. **(B)** Fiber type assignment based on the percent expression of four adult isoforms of MYH in 233 single muscle fibers. Fibers of each type were ranked by percentage purity. Pure and mixed fibers are combined in the heatmap. The total number of pure and mixed fibers of each type in the dataset is indicated. Each vertical line represents a single fiber. Slow-1 fibers were defined as pure when expressing >80% of MYH, 2A and 2X when expressing >70% of MYH2 and MYH1, respectively. The other fibers were defined as mixed-type. The adult isoform MYH4 (grey font) is only present in trace amount in human limb muscles. **(C)** Principal component analysis (PCA) of pure fibers (circles) and mixed-type fibers (dots), using only proteins expressed in all fibers. N=233 pure and mixed-type single fibers, 178 proteins. **(D)** PCA loadings, with proteins driving the separation of slow-1 fibers in blue and of fast 2A and 2X in black. Proteins annotated as mitochondrial are significantly enriched in slow fibers ( $p=1E-15$ ). N=233 single fibers, 178 proteins.

ORIGINAL UNEDITED MANUSCRIPT

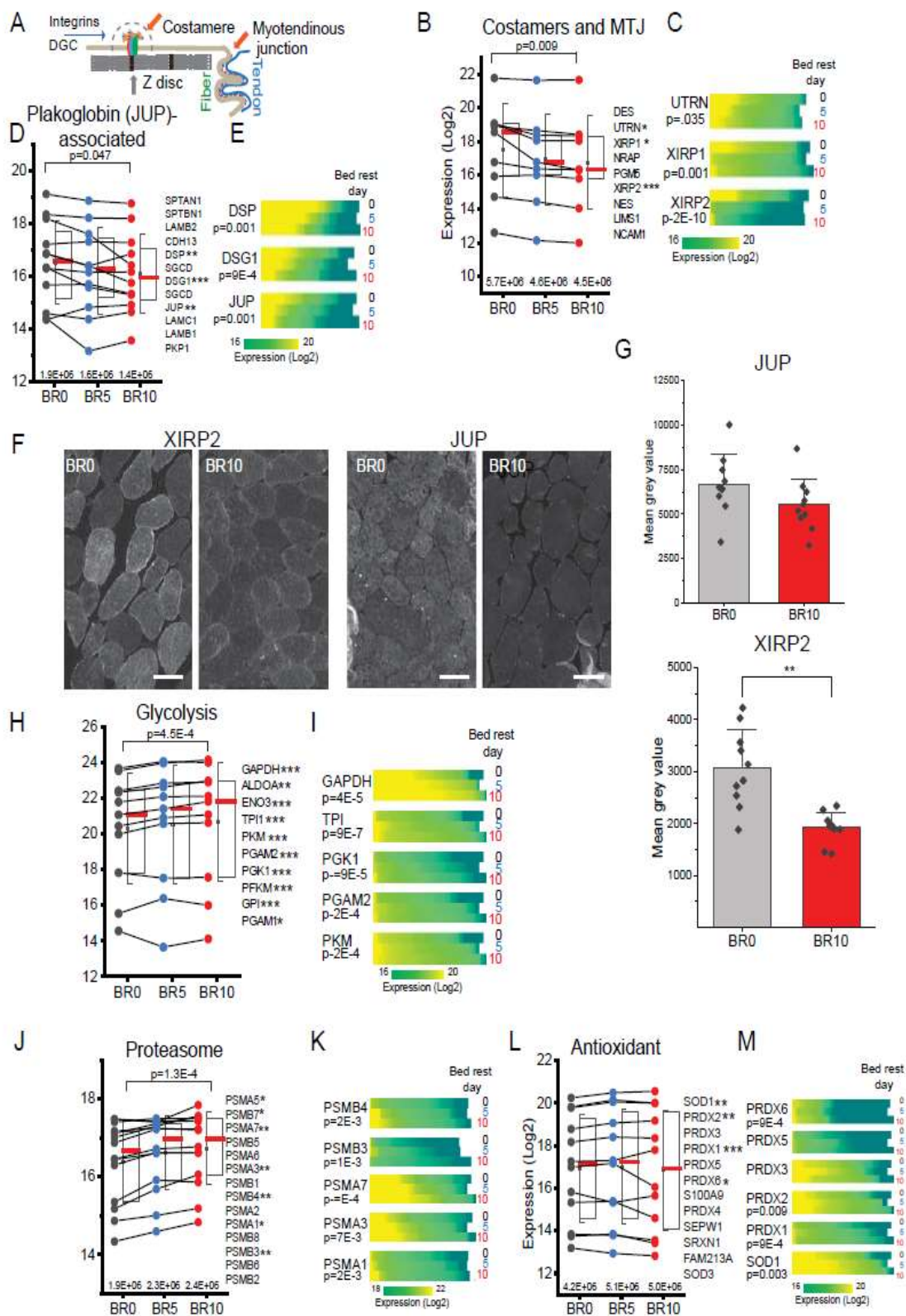


**Figure 2. Time-dependent proteomics features of muscle fiber disuse and unloading.**

**(A)** Schematic representation of costameres and myotendinous junction (MTJ) involved in muscle fiber- and muscle fiber-tendon adhesion. Some proteins mentioned in the text, such

ORCID

as XIRP1, XIRP2 and NRAP are located both at costameres and MTJ. **(B)** Trendlines with half boxplots of the expression of proteins enriched at the costameres and myotendinous junction (MTJ), with overall statistical significance on top (BR10 vs BR0, paired T-test). Box shows median in red, 75<sup>th</sup> and 25<sup>th</sup> percentile, whiskers SD. The protein list on the right is ordered by decreasing expression at BR10. Proteins with statistically significant expression difference in fibers before bed rest (BR0) and at BR10 are marked with asterisks (\* $p < 0.05$ , \*\* $p < 0.01$ , \*\*\* $p < 0.0001$ ). T-test,  $N = 78$  fibers at BR0 and 80 at BR10. Each fiber corresponds to one raw file and is considered as an independent experiment. The summed intensity of the proteins at each time point is shown above the x axis. **(C)** Heatmap of the expression in all fibers of three MTJ proteins with significant decrease upon unloading, UTRN, XIRP1 and XIRP2. Protein expression (LFQ intensity, Log2, color scale at bottom) is split into horizontal blocks, showing all fibers at each time of bed rest, as indicated on the right. BR0, 78 fibers, BR5 75, BR10 80. P value (T-test, BR10 vs BR0) is reported on the left. **(D)** Trendlines with half boxplots of the expression of proteins enriched at the costameres in complex with plakoglobin (JUP). See panel B. **(E)** Heatmap showing the expression in all fibers of three costameric proteins with significant decrease upon unloading (see panel C), DSP, DSG and JUP. See panel C. **(F)** Immunofluorescence analysis comparing the expression of XIRP2 and JUP at BR0 and BR10 in muscle biopsies of bed rest subjects. Representative images of the staining at BR0 and BR10 of the same subject. Brightness was digitally enhanced by an identical factor for paired images (XIRP2 300, XIRP1 150, JUP 100). **(G)** Bar graphs of median grey value in the stained biopsy of all subjects ( $N = 10$ ,  $> 50$  fibers/subject, T-test). **(H)** Trendlines with half boxplots of the expression of glycolytic enzymes. See panel B. **(I)** Heatmap showing the expression in all fibers of five glycolytic enzymes with significant increase in expression upon unloading. See panel C. **(J)** Trendlines with half boxplots of the expression of proteasome proteins. See panel B. **(K)** Heatmap showing the expression in all fibers of five proteasome subunits with significant increase in expression upon unloading See panel C. **(L)** Trendlines with half boxplots of the expression of proteins involved in protection from reactive oxygen species (Keywords annotation Antioxidant). Description as in A. **(M)** Heatmap showing the expression in all fibers of six antioxidant enzymes with significant increase in expression upon unloading. Description as in B.

ORIGINAL UNEDITED MANUSCRIPT

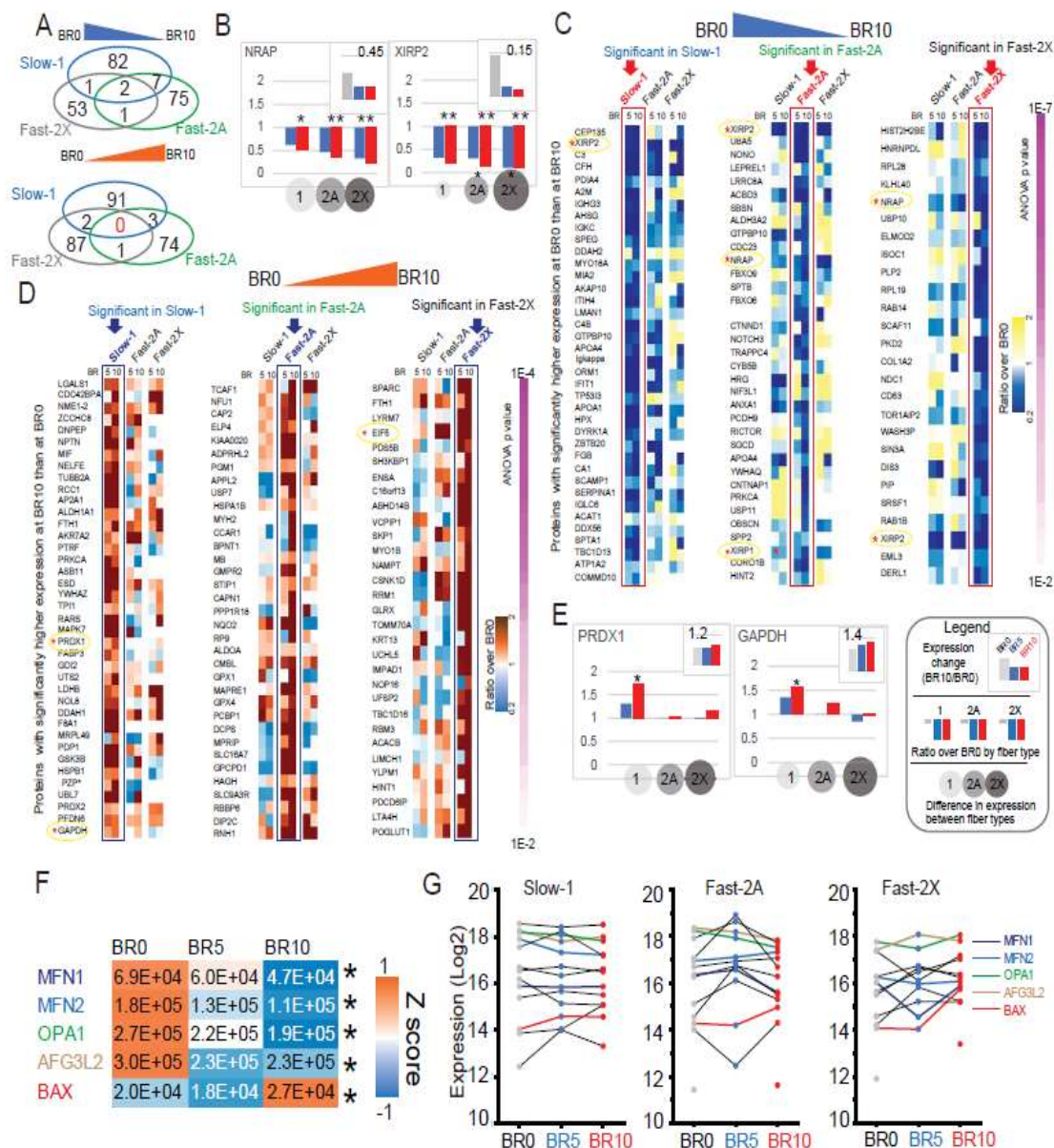


**Figure 3. Fiber type-specific effects of muscle unloading**

(A) Proteins with significantly lower (top) and higher (bottom) expression at BR10 compared to BR0. (B) Fiber type-resolved effects of muscle unloading on the two proteins significantly downregulated at BR10 in all three fiber types. The ratio between expression at BR10 and BR0 in all fibers (top graph), the ratio in individual pure fiber types (middle graph) and the relative expression in different fiber type (bottom circles) is shown as depicted in the legend next to panel E. BR0, grey bars; BR5, blue bars; BR10, red bars. T-test (\* $p < 0.05$ ). (C) Heatmap showing the expression ratio (BR10/BR0) of proteins with expression BR0>BR10 according to the color scale shown on the right. Only proteins with  $p \text{ value} < 0.01$  (ANOVA and post-hoc tests comparing only pure fibers of the same type) are shown in the heatmaps, the remaining proteins with  $0.01 < p \text{ value} < 0.05$  are listed in Table S8. The proteins are ranked by p value, as indicated on the right. For each fiber type, marked on top, the corresponding column in which the expression change is statistically significant is marked by a rectangle. (D) Heatmap showing the expression ratio (BR10/BR0) of proteins with expression BR0<BR10 according to the color scale shown on the right. See panel C and Table S8. (E) Fiber type-

ORCID

resolved effects of muscle unloading of two proteins upregulated by unloading only in type1-slow fibers. The ratio between expression at BR10 and BR0 in all fibers (top graph), the ratio in individual pure fiber types (middle graph) and the relative expression in different fiber type (bottom circles) is shown as depicted in the legend. BR0, grey bars: BR5, blue bars: BR10, red bars. T-test (\* $p < 0.05$ ). See detailed legend in panel E. **(F)** Heatmap with expression (LFQ (explain) intensity) of five proteins involved in mitochondrial network remodeling, with significantly different expression between BR0 and BR10 (marked by asterisk on the right). Color scale, Z score as indicated. BR0 N=78, BR5 N=75, BR10 N=80. **(G)** Profile plots by fiber type of the expression of protein annotated as “mitochondrial fusion” and “fission” (GOBP). The protein list, ordered by expression at day 10 in decreasing order, is shown on the right. The profiles and names of the five proteins with significant expression are labeled in colors as shown on the right.

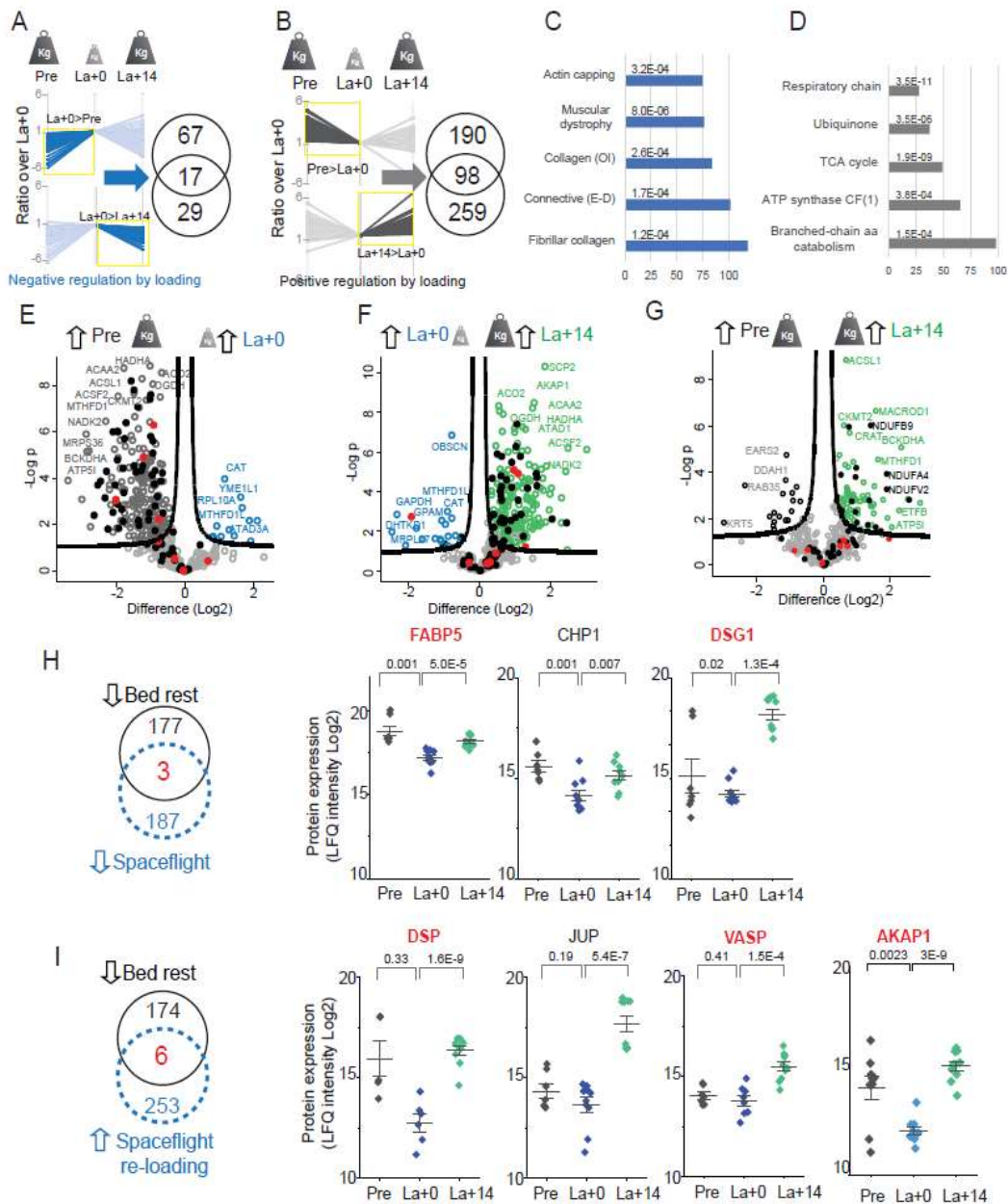


#### Figure 4. Effects of spaceflight on the whole muscle and mitochondrial proteome

**(A)** Left, Expression ratio (Log2) of proteins negatively regulated by weight load, with higher expression at La+0 compared to Pre-flight (ANOVA, significant in both astronauts). The darker line color and yellow box indicate the side with statistically significant expression difference (ANOVA and Tukey's HSD, N=5). Bottom, the same analysis for proteins decreasing their expression upon re-loading on Earth. Weight load changes during the phases of the mission are schematically represented on top. Right, number of proteins significantly up- and down-regulated shown in the corresponding profile plots, intersection shows the number of proteins with significant, opposite expression changes in both phases. **(B)** Same analysis for proteins positively regulated by weight load. **(C)** Annotation enrichments among proteins negatively regulated by weight load (intersection of Venn diagram in panel A, N=17 proteins). **(D)** Annotation enrichments among proteins positively regulated by weight load (intersection of Venn diagram in panel B, N=98 proteins). OI, osteogenesis imperfecta. E-D, Ehlers-Dannlos syndrome. **(E)** Comparison of the muscle mitochondrial proteome (Mitocarta 2) of astronauts from the biopsy before mission (Pre, Earth gravity, represented by large weighing weight) and on the day of landing after six months on the ISS (La+0, microgravity, represented by small weighing weight). A subset of proteins with large expression difference in the two conditions is labeled with their gene name. Respiratory chain proteins are marked by filled dots. Red dots, encoded by mtDNA. **(F)** Comparison of the muscle mitochondrial proteome from the biopsy before mission with that taken after 14 days of normal daily activity on Earth post-flight (La+14, see also E). **(G)** Comparison of the muscle mitochondrial proteome from the biopsy on the day of landing with that taken after 14 days of normal daily activity on Earth post-flight (see E, F). **(H)** Left, number of proteins with significant downregulation after bed rest (black) and after space flight (blue dashed), with 3 common proteins. Proteins lists derive from ANOVA (Bed rest, N= 83 and 80 single fibers. Astronauts, N= 10, 2 subjects, 5 technical replicates). Right, expression of the three common proteins in skeletal muscle before (Pre), on the day of landing (La+0) and 14 days after landing (La+14). N= 10, 2 subjects, 5 technical replicates. \*, p<0.05, \*\*, p<0.01, T-test. Protein name in red indicates common to panel I. **(I)** Left, number of proteins with significant downregulation after bed rest (left, red filled dots) and upregulated in astronauts after 14 days of normal daily activity on Earth post-flight (right, blue filled squares), with 6 common proteins. Right, expression of four of the six common proteins, the other 2 are in panel H (name in red). See panel H. **(J)** Column scatter detailing the expression of JUP and its interactor DSG1/desmoglein and DSP/desmoplakin in skeletal muscle before (Pre), on the day of landing (La+0) and 14 days after landing (La+14). N= 10, 2 subjects, 5 technical replicates. \*, p<0.05, \*\*, p<0.01, T-test. **(K)** Proteins with significant upregulation after bed rest (left, red filled dots) and downregulated in astronauts after 14 days of normal daily activity on Earth post-flight (right, blue filled squares). See panel E.

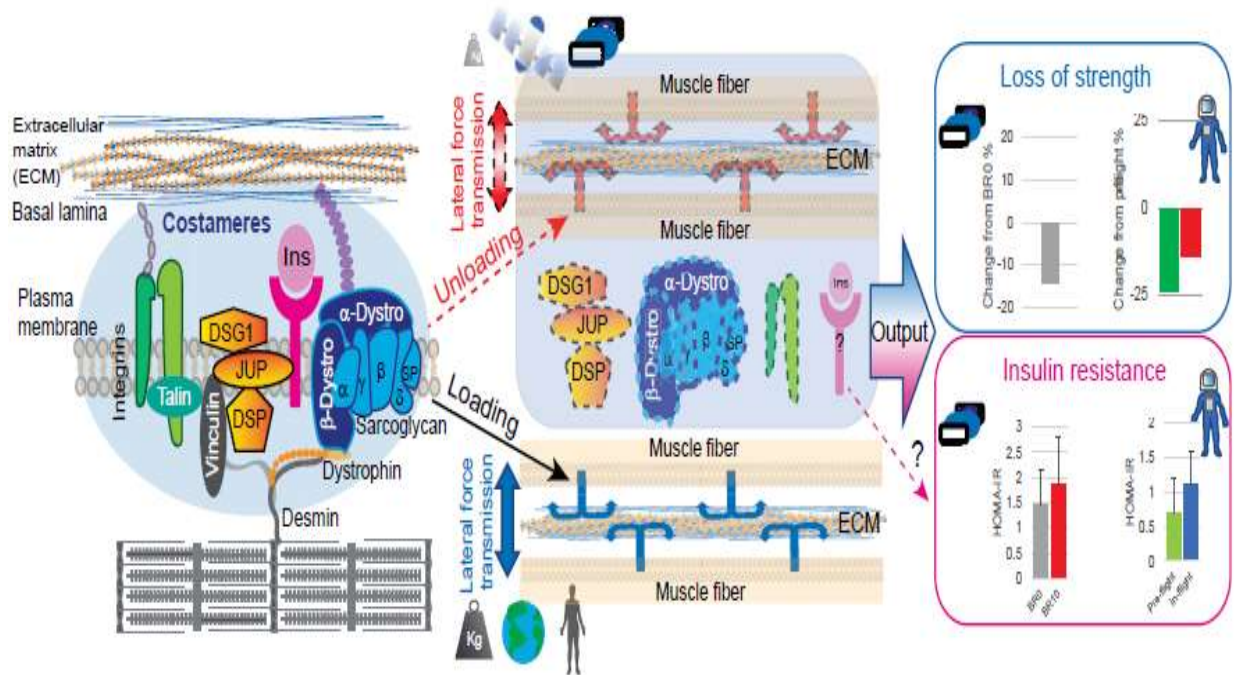


**Figure 5. Mechanical load controls the stability of costameric proteins.**

Both astronauts and volunteers undergoing bed rest experience decreased muscle strength (data derived with permission from References 5 and 9). We hypothesize that unloading, both on Earth and during spaceflight, leads to alteration of lateral force transmission by decreasing the expression of specific proteins located at the costameres (represented as anchors in central panel, see measured expression values in figures 2 and 4, S2 and S4, Tables S7 and S9), which couple the contractile apparatus to the extracellular matrix. Under normal weight load at Earth gravity, costameres allow for efficient transmission of contractile force from the muscle fibers to the ECM, and they prevent muscle contraction from damaging the sarcolemma. As a consequence of unloading, the expression of specific costameric proteins, thus the transmission of lateral force may result inefficient. Our data also show that the downregulation of plakoglobin (JUP) and its specific interactors desmoglein (DSG1) and desmoplakin (DSP) is strong both in bed rest and spaceflight. Plakoglobin is part of a complex that stabilizes the insulin receptor on the sarcolemma, so it will be of interest to further investigate its role in the development of insulin resistance during muscle inactivity on Earth and in space.